Afro-Asian Journal of Scientific Research (AAJSR)
المجلة الأفروآسيوية للبحث العلمي
E-ISSN: 2959-6505
Volume 4, Issue 4, 2026
Page No: 146-165
Website: https://aajsr.com/index.php/aajsr/index
SJIFactor 2024: 5.028 ISI 2025: 0.915 معامل التأثير العربي (AIF) 2025: 0.76

Regioselective Synthesis, Characterization, and Antimicrobial Evaluation of Novel Pyrazole, Hydrazone, and Azo-Benzoyl Acetone Derivatives under Catalyst-Free Conditions

Salma Swisse[1*], Abdalhamid Alarafi[2], Ali Alawami[3], Abdullah Gheath[4], Naowara Alarafi[5]
[1,4,5]Department of Chemistry, Faculty of Science, Benghazi University, Benghazi, Libya.
[2]Department of Chemistry, Faculty of Arts and Sciences, University of Benghazi, Al-Abyar, Libya.
[3]Department of Chemistry, Faculty of Humanities and Applied Science, Benghazi University, Tocra, Libya.

التخليق الانتقائي، التوصيف، والتقييم المضاد للميكروبات لمشتقات جديدة من البيرازول، الهيدرازون، وأزو بنزويل أسيتون في ظروف خالية من المحفزات

سالمة سويسي[1*]، عبد الحميد العرفي[2]، علي العوامي[3]، عبدالله غيث[4]، نوارة العرفي[5]
[1،4،5]قسم الكيمياء، كلية العلوم، جامعة بنغازي، بنغازي، ليبيا.
[2]قسم الكيمياء، كلية العلوم والآداب، جامعة بنغازي، الأبيار، ليبيا.
[3]قسم الكيمياء، كلية العلوم الإنسانية والتطبيقية، جامعة بنغازي، توكرة، ليبيا.

*Corresponding author: 8slma79y@gmail.com

Received: August 05 08, 2026	Accepted: October 13, 2026	Published: October 29, 2026

Copyright: © 2026 by the authors. Submitted for possible open access publication under the terms and conditions of the Creative Commons Attribution (CC BY) license (https://creativecommons.org/licenses/by/4.0/).

Abstract:
This study presents a catalyst-free, regioselective synthesis of a series of heterocyclic and azo-linked compounds derived from benzoyl acetone. The initial phase investigated the condensation of benzoyl acetone with hydrazine hydrate and ethylenediamine under varied molar ratios (1:1, 2:1, and excess) at room temperature. For the hydrazine series, reactions at 1:1 and 2:1 stoichiometries both yielded the same pyrazole product (I), while an excess of hydrazine produced a distinct hydrazone derivative (II). In contrast, the reaction with ethylenediamine consistently afforded a single product (VI) regardless of the molar ratio employed. The intermediate (II) was further functionalized via condensation with various aldehydes (1:1) to generate a new series of schiff bases (III, IV, V). In the final phase, benzoyl acetone was subjected to azo-coupling with a diazonium salt derived from 2,4-dichloro aniline to yield an azo-benzoyl acetone derivative. Subsequent reaction of this azo intermediate with hydrazine hydrate under different molar ratios surprisingly led to the same product (VII) in all cases, indicating a highly regioselective transformation. All synthesized compounds were characterized by melting point determination, TLC, and comprehensive spectroscopic techniques, including ^{1}H-NMR (with D_2O exchange), ^{13}C-NMR, and APT analyses. The antimicrobial activity of selected compounds (I, II, V, VI, and VII) was evaluated against three Gram-negative bacterial strains: Escherichia coli, Klebsiella pneumoniae, and Salmonella spp., and compared with standard antibiotics. Compound (I) demonstrated the highest antibacterial potency across all tested bacterial strains. At a 5% concentration, compound (VII) exhibited notable activity specifically against Salmonella spp. However,

compounds (II), (V), and (VI) showed no inhibitory effect against Salmonella spp., while compounds (II), (V), and (VII) were found to be inactive against K. pneumoniae. The results highlight the influence of structural modification on antimicrobial selectivity and position compound (I) as a promising lead for further development. To examine the binding interactions and possible binding modes of the synthesized compounds, molecular docking studies were conducted against dihydrofolate reductase (DHFR) from Klebsiella pneumoniae (PDB ID: 4OR7). With a docking score of −7.167 kcal/mol, compound VI had the best binding affinity among the tested compounds, while compound I had the lowest, with a score of −5.166 kcal/mol. Additionally, the electronic characteristics and global reactivity of the synthesized compounds were examined through Density Functional Theory (DFT) calculations. Compound VII had the smallest HOMO–LUMO energy gap (3.7239 eV), indicating relatively higher chemical reactivity, according to the computed frontier molecular orbital energies and global reactivity descriptors, which showed variations in the electronic characteristics and reactivity of the examined compounds.

Keywords: Benzoyl acetone, regioselective synthesis, hydrazones, Schiff bases, azo-coupling, antimicrobial activity, molecular docking, DFT.

الملخص:

تقدم هذه الدراسة توليفًا انتقائيًا موضعيًا وخاليًا من المحفزات لسلسلة من المركبات الحلقية غير المتجانسة والمرتبطة بروابط آزو، والمشتقة من بنزويل أسيتون. درست المرحلة الأولية تكثيف بنزويل أسيتون مع هيدرات الهيدرازين والإيثيلين داي امين بنسب مولية مختلفة (1:1، 2:1، وفائض) عند درجة حرارة الغرفة. بالنسبة لسلسلة الهيدرازين، أسفرت التفاعلات بنسب 1:1 و2:1 عن نفس ناتج البيرازول(I) ، بينما أنتج فائض الهيدرازين مشتق هيدرازون مميز .(II) في المقابل، أعطى التفاعل مع الإيثيلين داي امين باستمرار ناتجًا واحدًا (VI) بغض النظر عن النسبة المولية المستخدمة تمت إضافة مجموعات وظيفية إلى المركب الوسيط (II) عبر تكثيفه مع ألدهيدات مختلفة (بنسبة 1:1) لإنتاج سلسلة جديدة من قواعد شيف (III, IV, V) في المرحلة النهائية، خضع بنزويل أسيتون لتفاعل اقتران آزو مع ملح ديازونيوم مشتق من 2،4-ثنائي كلورو أنيلين لإنتاج مشتق آزو-بنزويل أسيتون. أدى التفاعل اللاحق لهذا المركب الوسيط الآزو مع هيدرات الهيدرازين بنسب مولية مختلفة، بشكلٍ مفاجئ، إلى نفس الناتج (VII) في جميع الحالات، مما يشير إلى تحول انتقائي موضعي عالي. تم توصيف جميع المركبات المُصنّعة من خلال تحديد نقطة الانصهار، والكروماتوغرافيا الطبقية الرقيقة، وتقنيات التحليل الطيفي الشاملة، بما في ذلك الرنين النووي المغناطيسي للبروتون (مع تبادل الديوتيريوم والأكسجين)، والرنين النووي المغناطيسي للكربون، وتحليل APT .وقد تم تقييم النشاط المضاد للميكروبات لمركبات مختارة (I, II, V, VI, and VII) ضد ثلاثة سلالات من البكتيريا سالبة الغرام: الإشريكية القولونية، والكلبسيلة الرئوية، والسالمونيلا، ومقارنتها بالمضادات الحيوية القياسية. أظهر المركب (I) أعلى فعالية مضادة للبكتيريا بين جميع السلالات البكتيرية المختبرة. عند تركيز 5% أظهر المركب (VII) نشاطًا ملحوظًا على وجه التحديد ضد السالمونيلا. ومع ذلك، لم تُظهر المركبات(II) ، (V)، و (VI)أي تأثير مثبط ضد السالمونيلا، بينما وُجد أن المركبات(II) ، (V) و (VII)غير فعالة ضد الكلبسيلة الرئوية. تُبرز هذه النتائج تأثير التعديل البنيوي على الانتقائية المضادة للميكروبات، وتُصنّف المركب (1) كعامل واعد للمساهمة في المزيد من التطوير. لفحص تفاعلات الارتباط وأنماط الارتباط المحتملة للمركبات المصنعة، أُجريت دراسات الإرساء الجزيئي ضد إنزيم ديهيدروفولات ريدوكتاز (DHFR) من كليبسيلا الرئوية (PDB ID: 4OR7) مع درجة إرساء قدرها 7.167- كيلو كالوري/مول، كان للمركب السادس أفضل ألفة ارتباط بين المركبات المختبرة، بينما كان للمركب الأول أدنى درجة حيث بلغت 5.166- كيلو كالوري/مول. بالإضافة إلى ذلك، تم فحص الخصائص الإلكترونية والتفاعلية العامة للمركبات المصنعة من خلال حسابات نظرية الكثافة الوظيفية (DFT) كان للمركب السابع أصغر فجوة طاقة بين أعلى مدار جزيئي مشغول (HOMO) وأدنى مدار جزيئي غير مشغول (LUMO) (3.7239 إلكترون فولت)، مما يشير إلى تفاعلية كيميائية أعلى نسبيًا وفقًا لطاقات المدارات الجزيئية الحدية المحسوبة ومؤشرات التفاعلية العامة والتي أظهرت اختلافات في الخصائص الإلكترونية وتفاعلية المركبات التي تم فحصها.

الكلمات المفتاحية: بنزويل أسيتون، التخليق الانتقائي الموضعي، الهيدرازونات، قواعد شيف، اقتران الآزو، النشاط المضاد للميكروبات، الإرساء الجزيئي، نظرية الكثافة الوظيفية.

Introduction:

Dicarbonyl compounds represent a cornerstone of modern synthetic and coordination chemistry due to their unique structural framework featuring two carbonyl groups separated by a single methylene unit. This arrangement imparts distinct chemical properties, most notably a pronounced keto-enol tautomerism and a highly acidic methylene group, enabling a wide array of versatile reactions including C-C bond formation via enolate chemistry and the synthesis of various heterocycles and Schiff base ligands [1-6]. Among these, benzoylacetone (1-phenylbutane-1,3-dione) is particularly significant. Its structure, which combines a phenyl ring with a 1,3-dicarbonyl system, provides enhanced resonance stability and a strong affinity for coordinating with transition metals, making it an essential precursor for more complex derivatives [7].

The synthesis of benzoylacetone, first achieved by Ludwig Claisen via a crossed Claisen condensation, has paved the way for its extensive use in synthesizing a diverse range of compounds with significant biological and pharmacological activities [8]. Derivatives of benzoylacetone, such as hydrazones, Schiff bases, and pyrazoles, have been widely reported to exhibit antibacterial, antifungal, anticancer, and anti-inflammatory properties [9-18]. This broad spectrum of activity, combined with the compound's utility as a chelating ligand, underscores its importance in the development of new therapeutic agents and functional materials. Given the substantial potential of benzoyl acetone derivatives in various scientific fields, this study aims to synthesize a novel series of such compounds. The synthesis will focus on the condensation of benzoyl acetone with different diamines, hydrazines, and subsequent reactions with various aldehydes and diazonium salts. All newly synthesized compounds will be characterized using standard spectroscopic techniques and evaluated for their *in vitro* antibacterial activities, contributing to the ongoing exploration of this versatile class of organic compounds.

Additionally, molecular docking studies were performed to investigate the binding interactions of the synthesized compounds with dihydrofolate reductase (DHFR) from Klebsiella pneumoniae (PDB ID: 4OR7). Docking analysis was employed to elucidate the binding modes and potential interactions of the compounds within the active site of the target protein. Furthermore, the optimized molecular structures and electronic properties of the synthesized compounds were examined using Density Functional Theory (DFT) calculations. Frontier molecular orbital energies (HOMO and LUMO) and global reactivity descriptors, including chemical hardness, chemical softness, chemical potential, electrophilicity, and nucleophilicity, were analyzed.

Material and methods:

Materials:

All chemicals were purchased from Sigma Aldrich (St. Louis, Mo, USA) and were used as received. Reactions were monitored on TLC (Chloroform /hexane). ^{1}H NMR spectra were carried out in the Centre for drug discovery research & development at ain shams university on Bruker 300 MHz with chemical shift (δ) expressed in ppm downfield from tetra methyl silane as an internal stander (δ TMS = 0) using CDCl3 as a solvent. The multiplicity of the signal is as following: s (Singlet), d (Doublet), t (Triplet), q (Quartet), m (Multiplet).^{13}C-NMR were measured in the Centre for drug discovery research & development at ain shams university on Bruker 75 MHz with internal reference TMS δ = 0. Melting points (m.p) of the synthesized compounds were measured in capillary tubes using Stuart scientific apparatus and are uncorrected.

Methods:

1. Reaction of benzoyl acetone with diamine compounds:

Benzoylacetone (0.01 mol) was dissolved in ethanol (10–15 mL), and hydrazine hydrate (0.01 mol) was added dropwise with continuous magnetic stirring at ambient temperature (25–30 °C). The progress of the reaction was monitored by TLC. Upon completion, the precipitated solid was collected by vacuum filtration, washed with cold ethanol to remove unreacted starting materials, and recrystallized from ethanol to afford **compound (I)** as a pure crystalline product. When benzoylacetone was used in excess (0.02 mol) with hydrazine hydrate (0.01 mol) under the same conditions, the product obtained was again **compound (I).**

In a separate experiment, the molar ratio was altered to 0.01 mol of benzoylacetone and 0.02 mol of hydrazine hydrate. The reaction was conducted under identical conditions, and the product was isolated following the same work-up procedure to furnish **compound (II)**.

Compound **(VI)** was synthesized following the same general protocol described above, employing benzoylacetone and ethylenediamine in three different molar ratios: 1:1, 1:2, and 2:1, respectively. In each case, the appropriate quantities of the two reactants were dissolved in ethanol (10–15 mL) and stirred at room temperature. The reaction was monitored by TLC until completion. The resulting precipitate was isolated by vacuum filtration, washed with cold ethanol, and recrystallized from ethanol to afford **compound (VI)** as a pure crystalline product in all three cases, indicating that the same product is formed irrespective of the stoichiometric ratio employed.

2. **Reaction of compound (II) with different aldehydes**:

Equimolar quantities of compound (II) (0.01 mol) and the selected aldehyde (0.01 mol) were dissolved in absolute ethanol (10–15 mL) and the resulting mixture was magnetically stirred at ambient temperature (25–30 °C). The reaction was monitored by TLC. After complete consumption of the starting materials the solid precipitate that formed was isolated by filtration under reduced pressure. The crude product was thoroughly washed with chilled ethanol (2 × 5 mL) to eliminate trace impurities, and subsequently recrystallized from hot ethanol to give the target compounds (III-V) as crystalline solids.

3. Reaction of diazinyl with hydrazine hydrate:

A 50 mL round-bottom flask was charged with 2-(2-(2,4-dichlorophenyl) hydrazineylidene)-1-phenylbutane-1,3-dione (0.01 mol) and dissolved in a minimum volume of absolute ethanol (10–15 mL). To this stirred solution, hydrazine hydrate (0.01 mol) was added dropwise at ambient temperature. The reaction mixture was continuously stirred at room temperature, and the progress was monitored by TLC. Upon completion of the reaction a solid precipitate began to form. The mixture was left to stir for an additional [50 minutes] to ensure complete precipitation. The resulting crude product was isolated by vacuum filtration, washed thoroughly with cold ethanol (2 × 5 mL) to remove any unreacted starting materials and soluble impurities, and subsequently air-dried. The purified product was obtained by recrystallization from hot ethanol, yielding compound VII as a yellow crystal.

4. Evaluation of Antibacterial Activity:

Bacterial Isolates:

The bacterial strains employed in this investigation comprised *Escherichia coli*, *Klebsiella pneumoniae*, and *Salmonella* spp. All isolates were obtained from [the stock culture collection of the Microbiology Department, Benghazi University]. The cultures were maintained on Nutrient Agar (Oxoid, Basingstoke, UK) slants at 4°C and sub cultured freshly onto Nutrient Agar plates at 37°C for 18–24 hours prior to each experiment to ensure optimal viability and purity.

Culture Medium:

Nutrient Agar (Oxoid, Basingstoke, UK) was utilized as the growth medium for both the propagation of bacterial isolates and the subsequent antimicrobial susceptibility testing. The medium was prepared according to the manufacturer's instructions by suspending the required amount of dehydrated powder in distilled water, followed by sterilization via autoclaving at 121°C for 15 minutes at 15 psi. The sterilized medium was then cooled to approximately 45–50°C prior to pouring into sterile Petri dishes.

Antibacterial Activity Assay:

The *in vitro* antibacterial activity of the synthesized compounds was evaluated using the agar well diffusion method as described by Perez et al. [19] with minor modifications. Briefly, bacterial inoculated were prepared by suspending overnight cultures in sterile normal saline (0.9% NaCl) to achieve a turbidity equivalent to a 0.5 McFarland standard (~1.5 × 10^8 CFU/mL). A sterile cotton swab was then used to uniformly spread the standardized bacterial suspension across the entire surface of pre-solidified sterile Nutrient Agar (Oxoid, Basingstoke, UK) plates.

Using a sterile corn borer (6 mm in diameter, matching the size of the standard antibiotic discs employed in the study), wells were aseptically punched into the agar medium. A fixed volume (100 µL) of each test compound solution, prepared at varying concentrations (e.g., 50, 100, and 200 µg/mL) in an appropriate solvent (e.g., dimethyl sulfoxide, DMSO), was introduced into the respective wells. The

plates were allowed to stand at room temperature for 30 minutes to facilitate pre-diffusion of the test compounds prior to incubation. Subsequently, the plates were incubated aerobically at 37°C for 24 hours in an incubator (Oxoid). Following the incubation period, antibacterial activity was assessed by measuring the diameter of the clear inhibition zones (including the well diameter) around each well using a digital vernier caliper, and the results were recorded in millimeters (mm). All assays were performed in triplicate, and the results were expressed as mean ± standard deviation (SD).

A positive control (e.g., gentamicin or ciprofloxacin, 10 µg/well) and a negative control (the solvent used for dissolution, e.g., DMSO) were included in each experiment to validate the assay conditions and to confirm the absence of solvent-induced inhibition.

Antibiotic Susceptibility Testing:

The antibiotic susceptibility profile of the bacterial isolates was determined using the standard Kirby-Bauer disc diffusion method in accordance with the Clinical and Laboratory Standards Institute (CLSI) guidelines [20]. Briefly, standardized bacterial suspensions (0.5 McFarland standard) were swabbed uniformly onto the surface of Mueller-Hinton Agar (or Nutrient Agar) plates. Commercially available antibiotic discs (Oxoid) containing predefined concentrations of various antimicrobial agents were aseptically placed onto the inoculated agar surface using sterile forceps. The discs were gently pressed down to ensure firm contact with the agar surface. The plates were incubated at 37°C for 24 hours. After incubation, the diameters of the inhibition zones were measured in millimeters and interpreted as sensitive (S), intermediate (I), or resistant (R) according to the CLSI breakpoint criteria [20]

5. Computational detail:

Ligands preparation:

Initial 3D configurations of the ligands were subjected to a pre-optimization stage relying on the Energy Minimize tool available in MOE 2024 [21]. Following partial charge determination, energy minimization was executed applying the Amber:EHT force field alongside a reaction field implicit solvation model (R-Field 1:80). This minimization process ceased once an RMS gradient limit of 0.1 kcal/mol/Å² was achieved. Next, density functional theory (DFT) calculations using the B3LYP/6-31G basis set [22, 23] were carried out on the structures to locate their most stable conformations, which subsequently served for determining global reactivity descriptors via Gaussian 09 [23]. Standard convergence endpoints for maximum force, root-mean-square (RMS) force, maximum displacement, and RMS displacement were successfully satisfied as default settings. Furthermore, vibrational frequency computations yielded exclusively positive values across the drugs, providing clear confirmation of their stability [24].

Receptor preparation:

The crystallographic structure corresponding to Klebsiella pneumoniae dihydrofolate reductase, registered under PDB ID: 4OR7, was downloaded directly from the Protein Data Bank. Prior to downstream procedures, structural water molecules alongside the NAP cofactor were eliminated. The protein target was optimized utilizing the QuickPrep function embedded in MOE 2024, which encompasses sequence preservation, neutralization of the structure, 3D protonation via Protonate3D (incorporating ASN/GLN/HIS flips), and the inclusion of missing hydrogen atoms. Subsequent energy minimization was carried out under specific receptor tethering restraints (Strength: 10, Buffer: 0.25 Å; fixed atoms > 8.0 Å) until reaching the 0.1 kcal/mol/Å² RMS gradient threshold.

Molecular docking:

Scoring and docking procedures were executed making use of the Molecular Operating Environment software, MOE (Molecular Operating Environment (MOE), 2024). The structural coordinates for Klebsiella pneumoniae dihydrofolate reductase (PDB entry: 4OR7) [25] possess a resolution of 1.76 Å. Generally, resolutions falling inside the 1.5 to 2.5 Å window are deemed suitable for reliable docking investigations [26]. Validation of molecular docking outcomes typically relies on two key benchmarks: root-mean-square deviation (RMSD) values approaching 2.0 Å coupled with energy scores equal to or lower than -7 [27].

Global reactivity descriptors:

Conceptual density functional theory (DFT) allows for the derivation of global reactivity indices, which represent vital metrics for evaluating the kinetic stability and chemical reactivity profiles of compounds [28]. These descriptors comprise the energy of the highest occupied molecular orbital (EHOMO), the energy of the lowest unoccupied molecular orbital (ELUMO), energy gap (ΔE), global electrophilicity (ω), chemical potential (μ), chemical hardness (η), chemical softness (S), and nucleophilicity (N) [29]. Computation of these indices at **the B3LYP/6-31G level followed these expressions:**

- Δ E = ELUMO-EHOMO
- $\omega=\mu^2/2\ \eta$
- μ= (ELUMO+EHOMO)/2
- η = (ELUMO- EHOMO)/2
- S=1/ (2 η)
- N=EHOMO(Nucleophile) – EHOMO (TCE)

Within the framework of this research, these global reactivity parameters were specifically evaluated for compounds I, II, V, VI, and VII.

Results and discussion:

Results:

- ***(3- methyl-5-phenyl-1H- pyrazole ($C_{10}H_{10}N_2$) (I):*** Mol.wt. 158 g/mol, yield 33 % as a white solid, m. p 129-131 °C. ^{1}H NMR($CDCl_3$) δ = 2.25 (s, 3H, CH3), 6.4 (s, 1H, CH), 7,28 (t, 1H, CH), ,7.75 (d, 2H, 2CH), 7,75 (t, 2H,2CH), 12.5 (s, 1H, NH).
- ***4-hydrazineyl-4-phenylbut-3-en-2-ylidene) hydrazine($C_{10}H_{14}N_4$) (II):*)**: yield 77 % as a white solid, p.m., 129-130 °C. ^{1}H NMR ($CDCl_3$) δ = 2.3 (S, 3H, CH_3), 6.4 (S, 1H, CH), 6,39(S, 1H, CH), 6.6(S, 1H, NH), 7.2-7.4 (m, 3H, Ar-H) 7.3 (S, 1H, CH), 3.29 (m, 4H, Ar-H), 7.4 (d, 2H, CH_2), 7.74-7.9 (dd, 2H, Ar-H).
- ^{13}C NMR ($CDCl_3$) δ = 7 (1C), 97 (1C)، 121.2(2C)، 123.69-123.9 (2C) (1C)، 123.9-124 (2C), 126, 138 (C=N), 144 (NH-C=C).
- ***1,2-bis((E)-3phenylallylidene) hydrazine($C_{18}H_{16}N_2$) (III):*** yield 61.2 % as a yellow solid, p.m., 155-156 °C. ^{1}H NMR ($CDCl_3$) δ = 7.1-7.13(m, 2H, CH), 7.45 (d, 1H, CH), 7.46 (m, 4H, ArH), 7.54 (S, 2H, NH_2),7.42 (d, 1H, CH) ,8.43 (t, 1H, CH).
- ^{13}C NMR ($CDCl_3$) δ =72 (1C), 120 (Ar), 130, 139, 158.
- ***4,4-(hydrazine-1,2-diylidenebis (methaneyllidene)) bisN,Ndimethylaniline($C_{18}H_{22}N_4$) (IV):*** yield 56.8 % as a yellow solid, p.m., 268-270°C.
- ^{1}H NMR ($CDCl_3$) δ =3.09 (S, 12H, 4CH_3), 6.75 (d, 4H, Ar-H), 7.76 (d, 4H, Ar-H), 8.62 (S, 2H, CH=N).
- ^{13}C NMR ($CDCl_3$) δ = 40 (4C)، 111.8 (4C)، 121.8 (2C)، 130.2 (4C)، 152.3 (2C)، 160.6 (2C).
- ***(2,2'-hydrazine-1,2-diylidenebis(methaneylylidene)diphenol ($C_{14}H_{12}O_2N_2$) (V):*** yield 41.4 % as a yellow solid, p.m., 220-222°C.
- ^{1}HNMR ($CDCl_3$) δ = 6.94-6.99 (m, 4H, CH), 7.36-7.40 (m, 2H, CH), 7.66-7.68 (m, 2H, CH), 8.97 (S, 2H, CH), 11.17 (S ,2H, OH).
- ^{13}CNMR ($CDCl_3$) δ =116.99 (2C),118.6 (2C),120 (2C),131.4 (2C),133.7 (2C),159.2 (2C),163.4 (2C).
- ***3,3'-(ethane-1,2-diylbis(azaneylylidene))bis(1-phenylbutan-1-one-1-ol) ($C_{22}H_{24}N_2O_2$) (VI):*** yield 11.5 % as a white solid, p.m., 184-186°C. ^{1}H NMR($CDCl_3$) δ = 2-2.22 (S, 6H, 2CH_3), 3.59-3.61 (S, 2H, CH_2), 5.72 (S, 1H, CH), 7.28-7.54 (m, 3H, CH), 7.85-7.91 (d ,2H, CH_2), 11.59 (S, 1H, 2OH).
- 13CNMR(CDCl3) δ = 19.26 (1C), 43.79 (2CH), 93 (1C), 126-130 (3C), 140 (C), 164.8 (C=N), 188 (1C).
- **2.5.1*-4-(2,4-dichlorophenyl) hydrazineyl)-3-methyl-5-phenyl-1H-pyrazole) ($C_{16}H_{12}N_4Cl_2$) (VII):***
- Mol.wt:260 g/mol yield 11 % as a yellow solid, m.p., 266-267°C.
- ^{1}H NMR ($CDCl_3$) δ = 2.50-2.53 (s, 3H, CH3), 7.45-7.47 (s, 1H, CH), 7.50-7.56 (m, 3H, CH), 7.62-7.64 (s, 1H, CH), 7.83-7.84(d, 1H, CH), 8.0-8.02 (d,2H, CH), 13.5 (s, 1H, NH).

Table (1): The results obtained from docking validation with Receptor 4OR7

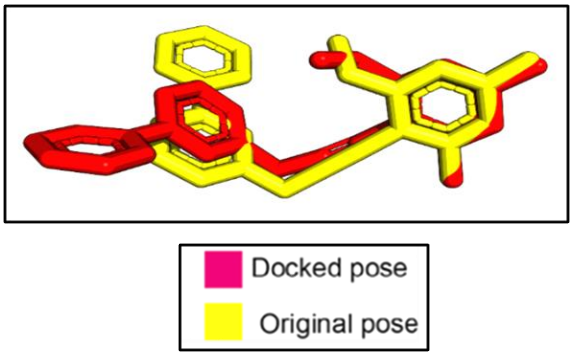
rotei Protein n	PDB ID	RMSD (Å)	Superimposition plot	
Dihydrofolate reductase (K. pneumoniae)	4OR7	1.365		

Table (2): The results obtained from docking of Ligands with 4OR7

Ligand	S score (kcal/mol)	RMSD (Å)	Atom of compound	Atom of receptor	Involved receptor residues	Type of interaction bond	Distance (Å)	E(kcal/mol)
Ref	-7.891	1.365	N3 9 NAD 12 NAD 12 NAE 17 NAE 17 N3 9 N3 9 NAD 12 NAD 12 6-ring	OD2 O OD1 O O OD1 OD2 OD1 OD2 6-ring	ASP 27 ALA 6 ASP 27 ILE 5 ILE 94 ASP 27 ASP 27 ASP 27 ASP 27 PHE 31	H-donor H-donor H-donor H-donor H-donor Ionic Ionic Ionic Ionic pi-pi	2.75 3.09 3.00 3.00 2.97 3.51 2.75 3.00 3.64 4.06	-7.4 -0.6 -8.0 -2.6 -1.7 -1.9 -6.4 -4.4 -1.4
I	-5.166	0.8015	N 1 5-ring	O CA	ILE 94 ALA 6	H-donor pi-H	2.93 3.70	-3.4 -0.5
II	-5.741	1.049	N 26 N 26	O O	ALA 7 ILE 14	H-donor H-donor	2.89 3.17	-2.1 -1.4
V	-5.998	1.727	6-ring 6-ring	CA CA	ALA 6 GLY 15	pi-H pi-H	3.59 4.75	-0.6 -0.6
VI	-7.167	1.666	6-ring	OG1	THR 46	pi-H	4.28	-0.6
VII	-6.244	1.568	6-ring 6-ring	OG1 6-ring	THR 46 PHE 31	pi-H pi-H	3.99 3.69	-0.5

Table (3): 2D,3D interaction of the docking Reference Ligand with 4OR7

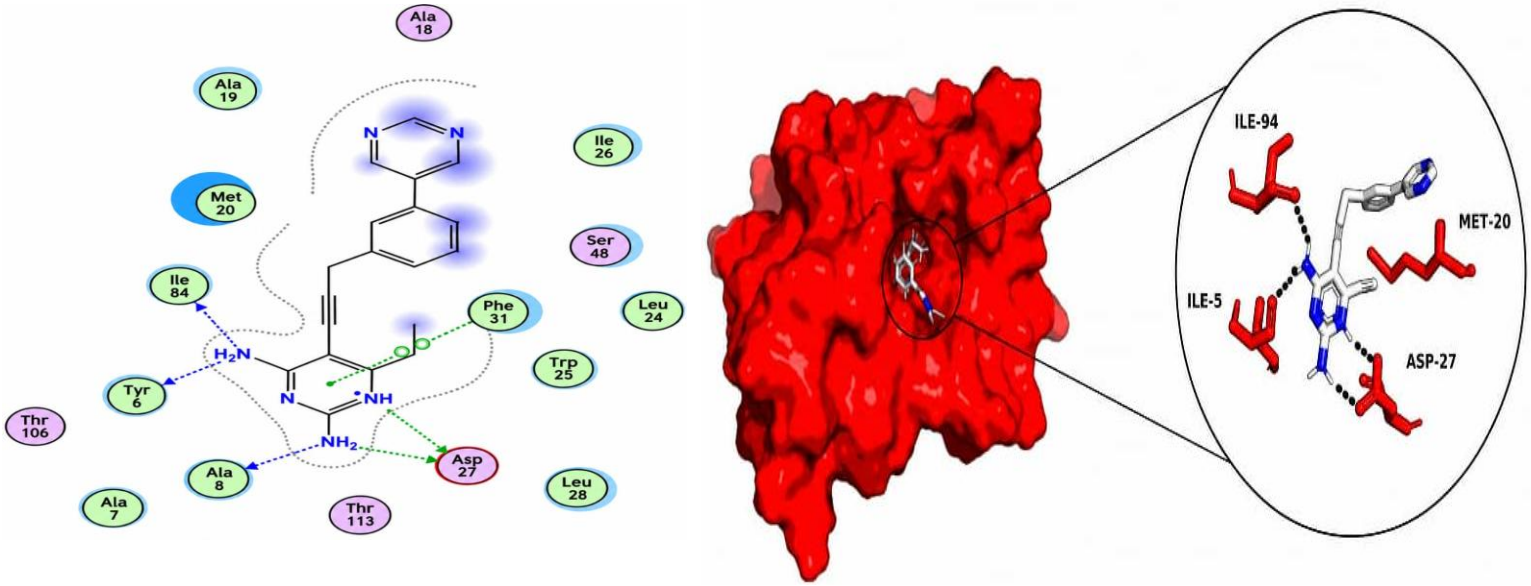
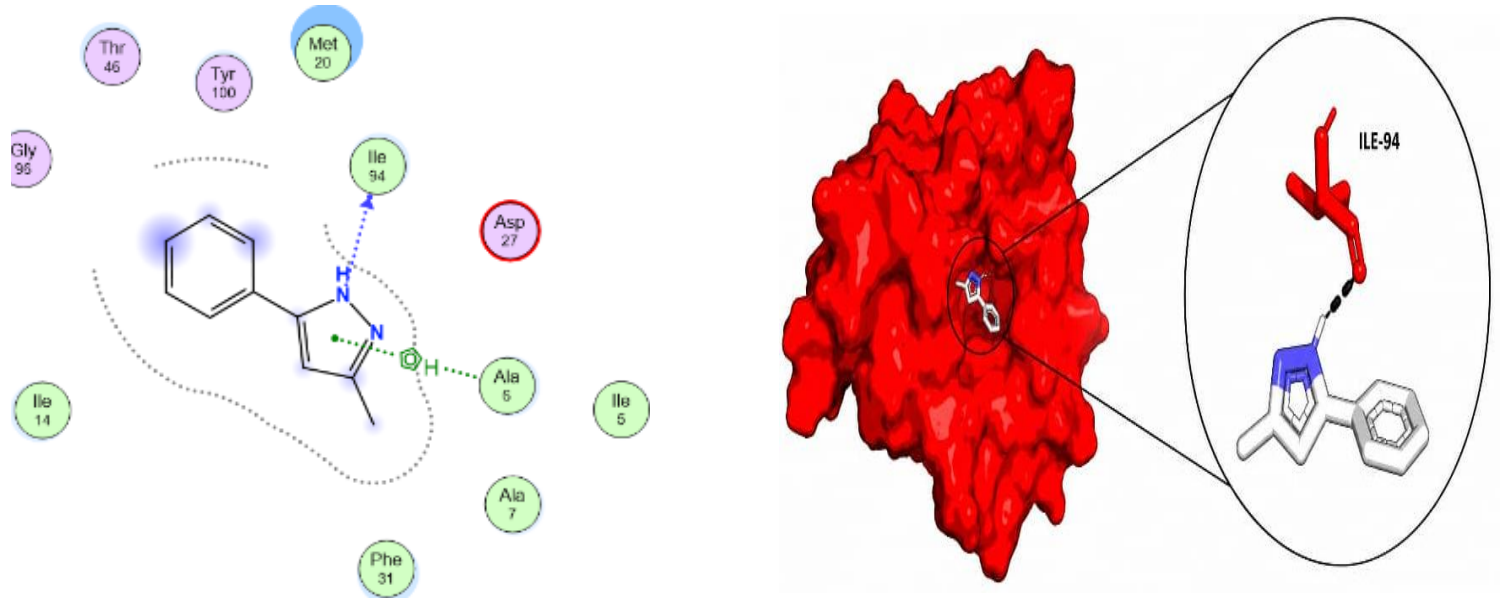
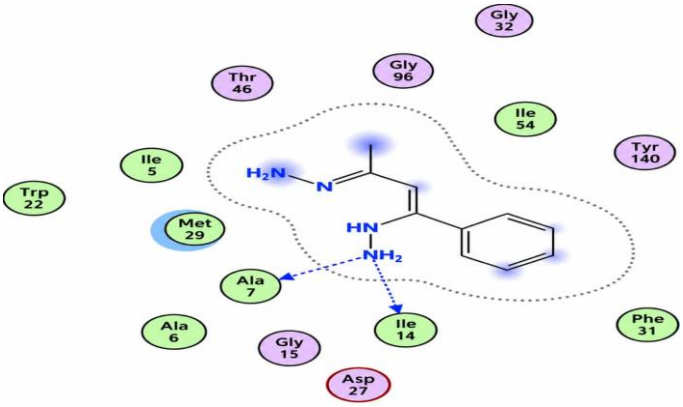
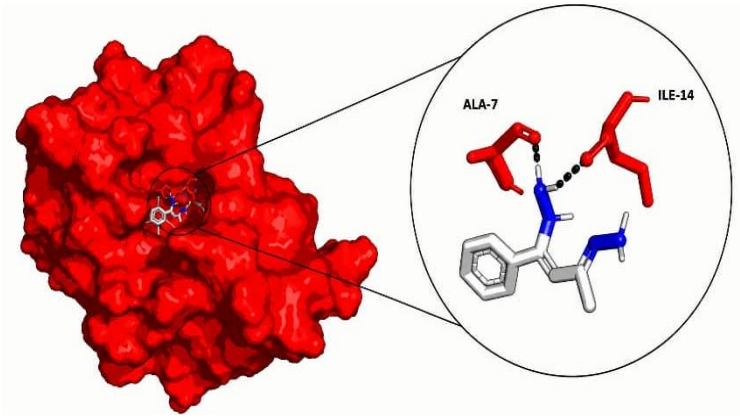


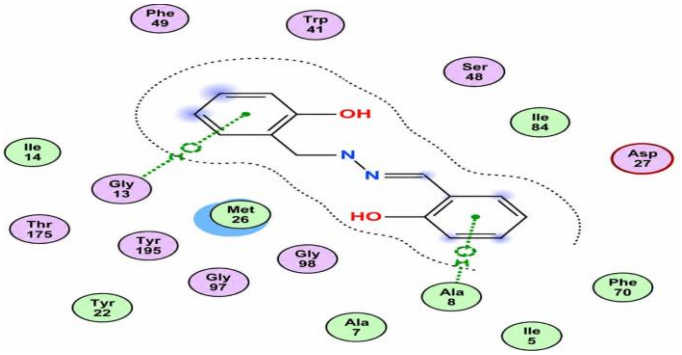
Table (4): shows the 2D and 3D interaction between ligand I,II,V,VI,VII OF 4OR7 Receptor

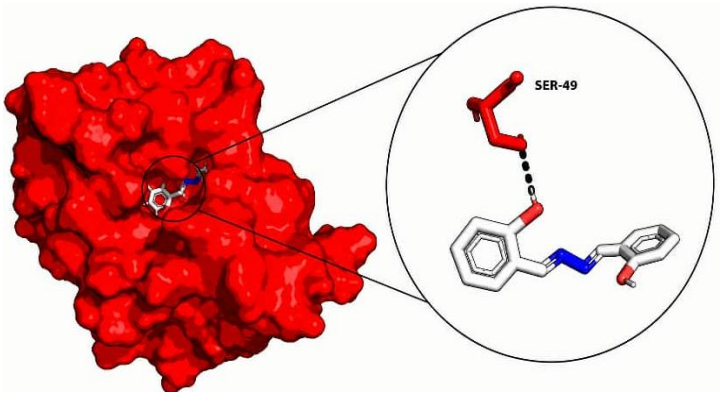
2D **3D**

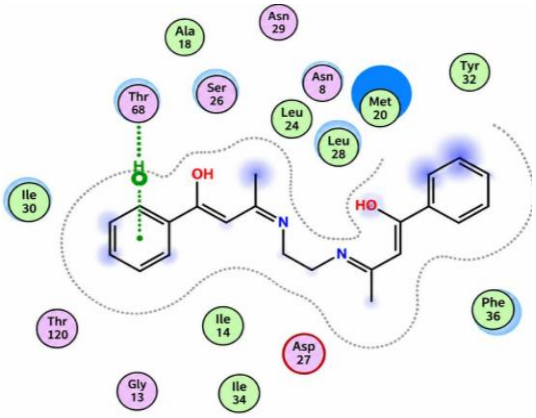


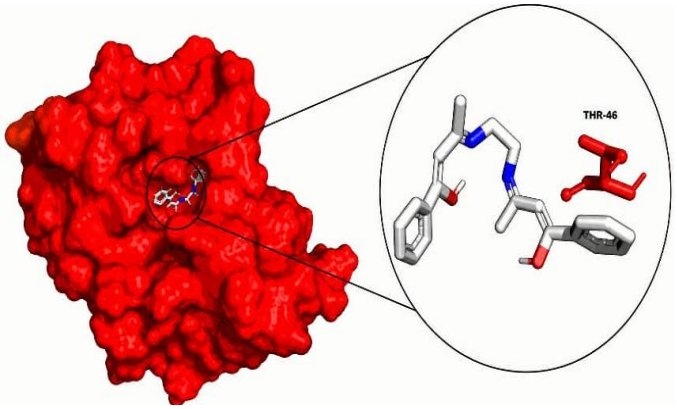

Gly 32
Gly 96
Thr 46
Ile 54
Tyr 140
Ile 5
Trp 22
Met 29
Ala 7
Ala 6
Gly 15
Ile 14
Phe 31
Asp 27

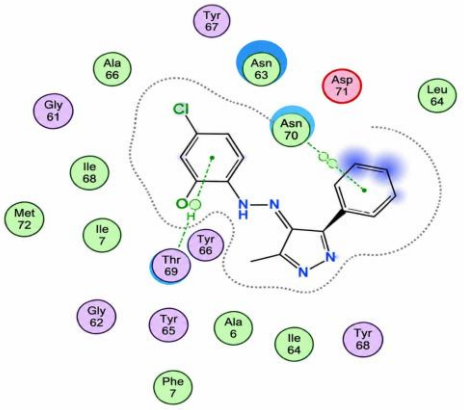

ALA-7
ILE-14


Phe 49
Trp 41
Ser 48
Ile 84
Ile 14
Asp 27
Gly 13
Met 26
Thr 175
Tyr 195
Gly 98
Gly 97
Ala 8
Phe 70
Tyr 22
Ala 7
Ile 5


SER-49


Ala 18
Asn 29
Ser 26
Asn 8
Tyr 32
Thr 68
Met 20
Leu 24
Leu 28
Ile 30
Phe 36
Thr 120
Ile 14
Asp 27
Gly 13
Ile 34


THR-46



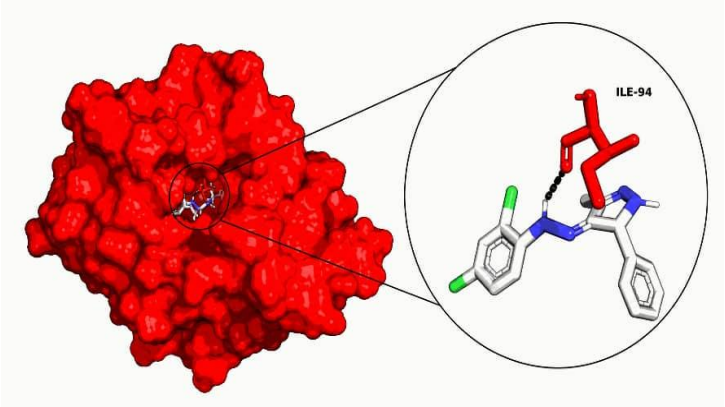
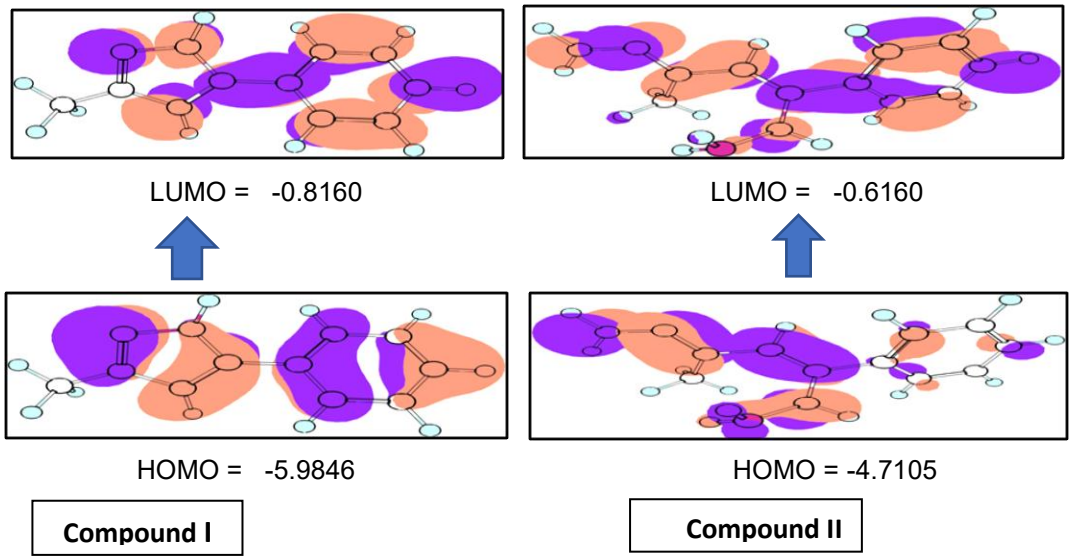


Table (5): HOMO and LUMO energy, energy gap ΔE and global reactivity indices μ, ω, η and N for Compounds.

Compound	HOMO (eV)	LUMO (eV)	ΔE (eV)	η (eV)	S (eV)	μ (eV)	ω (eV)	N (eV)
I	-5.9846	-0.8160	5.1686	2.5843	0.1934	-3.4003	2.2369	2.6713
II	-4.7105	-0.6160	4.0945	2.0472	0.2442	-2.6632	1.7322	3.9454
V	-5.6564	-1.7279	3.9285	1.9642	0.2545	-3.6921	3.4700	2.9995
VI	-5.4090	-1.5594	3.8496	1.9248	0.2597	-3.4842	3.1534	3.2469
VII	-5.3108	-1.5869	3.7239	1.8619	0.2685	-3.4488	3.1941	3.3451

Notes: the HOMO energy -8.6559 eV. of the reference system (TCE) had been calculated at DFT/B3LYP 6-31 G.



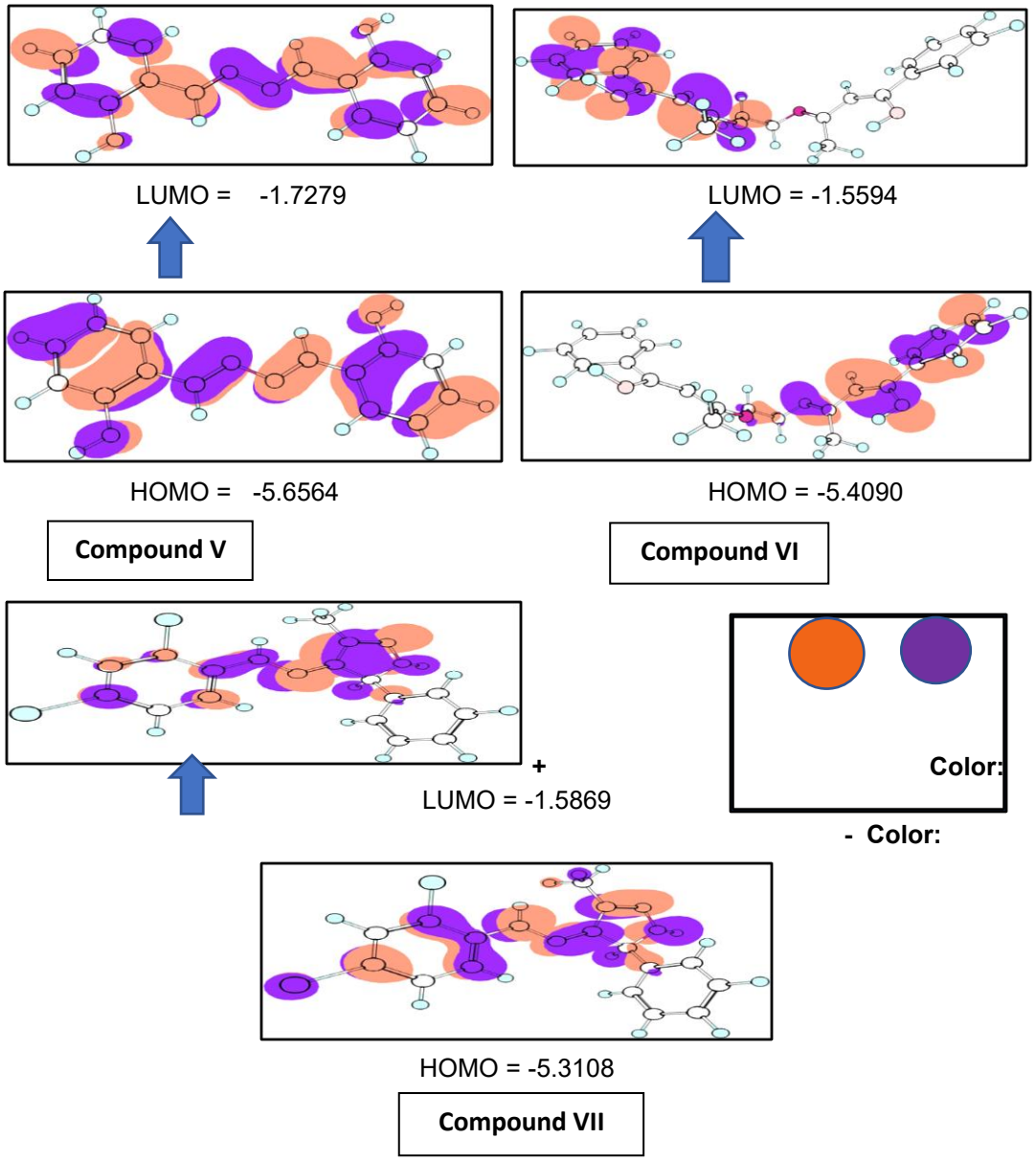
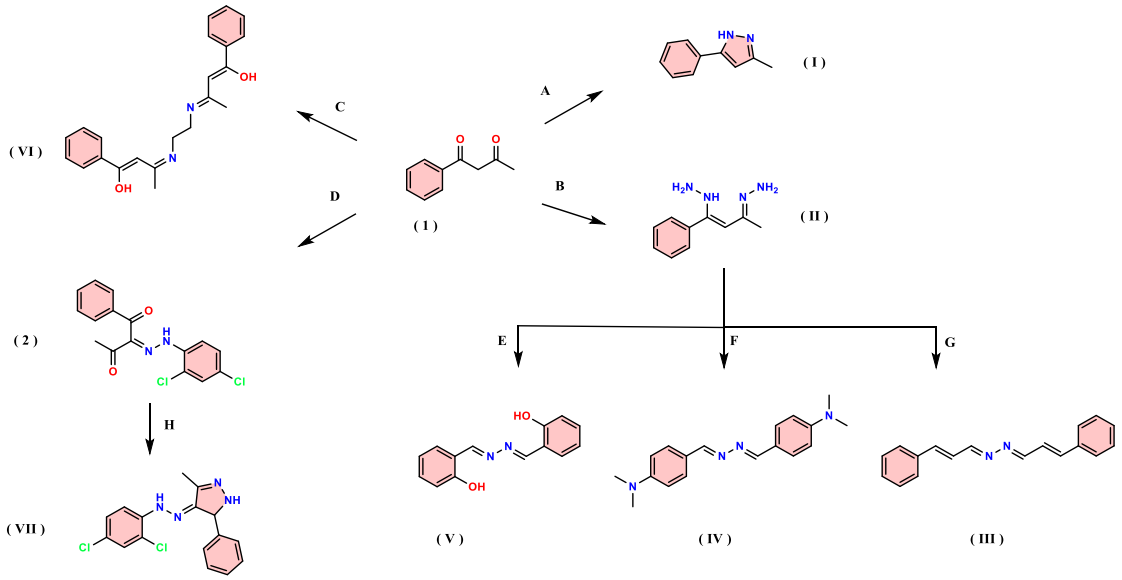


Figure (1): HOMO- LUMO Energy Gap

Discussion:

Benzoyl acetone (1) possesses multiple reactive sites that render it a versatile precursor for heterocyclic synthesis. The molecule contains two chemically distinct carbonyl groups an aromatic ketone and an aliphatic ketone along with an acidic methylene group and a methyl substituent. This structural complexity provides opportunities for regioselective transformations depending on the reaction conditions and the nature of the nucleophilic reagent employed. The reaction of benzoyl acetone with hydrazine hydrate and ethylenediamine were investigated under various stoichiometric ratios to exploit the differential reactivity of the carbonyl groups and to direct the reaction toward specific products (Scheme 1).



A= 1:2 and 2:1 Hydrazine (EtOH / RT), B = excess Hydrazine (EtOH / RT), C =1:2, 2:1 and excess ethylenediamine (EtOH / RT), D = Conc.HCl/ $NaNO_2$, E = salicylaldehyde (EtOH / RT), F= N, N-dimethylbenzaldehyde (EtOH / RT), G = cinnamaldehyde (EtOH / RT), H = 1:2, 2:1 and excess Hydrazine (EtOH / RT)

Scheme (1): The reaction of benzoyl acetone with hydrazine hydrate and ethylenediamine

When benzoyl acetone was treated with hydrazine hydrate in 1:1 and 2:1 molar ratios, the reaction exclusively afforded the pyrazolone derivative (I) in both cases. This observation indicates that the initial nucleophilic attack preferentially occurs at the more electrophilic aliphatic carbonyl carbon, followed by rapid intramolecular cyclization involving the methylene group to form the five-membered heterocyclic ring. The formation of the same product regardless of whether one or two equivalents of benzoyl acetone are employed suggests that the pyrazole ring formation is thermodynamically favored and proceeds through a kinetically controlled pathway that is not perturbed by an excess of the dicarbonyl component. The structural assignment of compound (I) was unequivocally established by comprehensive spectroscopic analysis. The ^{1}H NMR spectrum exhibited characteristic signals including a sharp singlet at δ 2.25 ppm integrating for six protons corresponding to two methyl groups, an olefinic proton signal at δ 6.4 ppm integrating for two protons, and complex aromatic proton resonances in the region δ 7.27-7.75 ppm. The downfield signal at δ 12.5-12.88 ppm, which disappeared upon D_2O exchange, was assigned to the NH proton, confirming the presence of the pyrazole NH moiety. The ^{13}C NMR spectrum further corroborated the proposed structure with appropriate chemical shifts for the pyrazole ring carbons and the aromatic system.

In contrast, when hydrazine hydrate was used in excess as both reagent and solvent, the reaction proceeded to give compound (II), 4-hydrazineyl-4-phenylbut-3-en-2-ylidenehydrazine. This product results from the condensation of both carbonyl groups with hydrazine, forming a conjugated hydrazone system. The ^{1}H NMR spectrum of compound (II) displayed a singlet at δ 2.35 ppm corresponding to the methyl group, an olefinic proton at δ 6.38 ppm, and aromatic protons appearing as multiplets in the region δ 7.28-7.87 ppm. The presence of NH and NH_2 protons was confirmed by D_2O exchange experiments, which revealed signals at δ 8.40 ppm that disappeared upon deuteration. The ^{13}C NMR spectrum showed the methyl carbon at δ 67 ppm and the olefinic carbon at δ 97.7 ppm. The aromatic carbons appeared as three distinct signals at δ 121.0, 123.6, and 124.1 ppm, each integrating for two carbon atoms, while a signal at δ 125.0 ppm corresponded to one aromatic carbon. Three quaternary carbons were observed at δ 126.0, 138.7, and 144.5 ppm, consistent with the proposed hydrazone structure. The divergent reactivity observed with hydrazine hydrate can be rationalized by considering the relative electrophilicity of the two carbonyl groups and the stability of the intermediate adducts. At equimolar or 2:1 ratio, the aliphatic ketone, being more electrophilic, undergoes preferential hydrazone formation. The resulting hydrazone intermediate then undergoes intramolecular cyclization through

attack of the hydrazine NH_2 group on the adjacent carbonyl, followed by dehydration to yield the aromatic pyrazole ring. In the presence of excess hydrazine, however, both carbonyl groups are converted to hydrazone functionalities, and the resulting bis-hydrazone is stabilized by extensive conjugation, preventing cyclization.

The reaction of benzoylacetone with ethylenediamine was investigated under three different molar ratios (1:1, 1:2, and 2:1). Remarkably, in all cases, the same product (VI) was obtained, indicating a highly selective transformation that is insensitive to stoichiometric variations. The formation of a single product from both 1:1 and 2:1 ratio suggests that the ethylenediamine-benzoyl acetone adduct undergoes rapid and irreversible conversion to a stable product that precludes further reaction.

The proposed mechanism involves initial nucleophilic attack of one amino group of ethylenediamines on the aliphatic carbonyl of benzoylacetone. The resulting imine intermediate then tautomerizes to the enamine form, which subsequently undergoes intramolecular hydrogen bonding and stabilization through conjugation with the adjacent carbonyl. The second amino group remains unreacted, possibly due to steric hindrance or the formation of a stable six-membered chelate ring through intramolecular hydrogen bonding that reduces its nucleophilicity.

The ^{1}H NMR spectrum of compound (VI) exhibited a singlet at δ 2.24 ppm integrating for six protons corresponding to two methyl groups, a singlet at δ 3.6 ppm for the methylene protons, an olefinic proton at δ 5.7 ppm, and aromatic protons appearing as two sets of signals at δ 7.3 ppm (3H) and δ 7.8 ppm (2H). The presence of a tautomeric hydroxyl group was confirmed by a signal at δ 11.6 ppm, which disappeared upon D_2O exchange. The ^{13}C NMR spectrum showed the methyl carbons at δ 14 ppm, the methylene carbon at δ 40 ppm, the olefinic carbon at δ 92 ppm, and aromatic carbons in the expected region. Quaternary carbons were observed at δ 139, 160, and 182 ppm, consistent with the proposed structure.

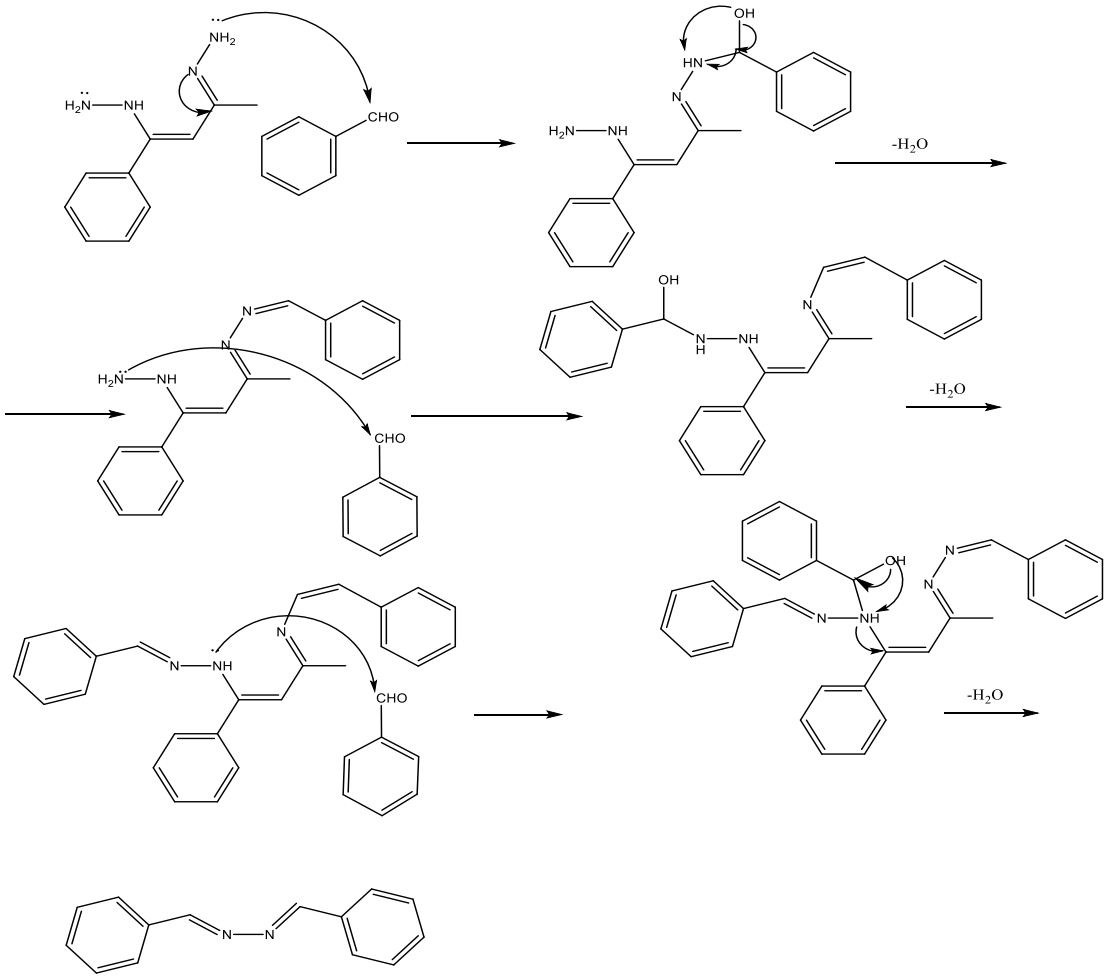
The presence of a free amino group in compound (II) provided an opportunity for further functionalization through condensation with various aldehydes to generate Schiff base derivatives. However, the reaction of compound (II) with cinnamaldehyde unexpectedly yielded compound (III), 1,2-bis((E)-3-phenylallylidene) hydrazine, which lacked the benzoyl acetone moiety entirely. This surprising result was confirmed by the absence of methyl and acidic protons in the ^{1}H NMR spectrum, which would be characteristic of the benzoyl acetone fragment.

The ^{1}H NMR spectrum of compound (III) showed signals at δ 7.08 ppm corresponding to the olefinic protons of cinnamaldehyde, while other protons appeared as multiplets in the region δ 7.20-7.80 ppm. The imine proton (H-C=N) was deshielded and appeared at δ 8.40 ppm. The ^{13}C NMR spectrum showed all carbons in the unsaturated region, with signals at δ 120-124 ppm for the aromatic carbons and a signal at δ 160 ppm for the carbon attached to nitrogen.

Similarly, the reaction of compound (II) with N, N-dimethylbenzaldehyde gave compound (IV), 4,4'-((1E,1'E)-hydrazine-1,2-diylidenebis(methaneylylidene)) bis (N, N-dimethylaniline), and the reaction with salicylaldehyde afforded compound (V), (2,2'-hydrazine-1,2-diylidenebis(methaneylylidene)) diphenol. In both cases, the spectroscopic data confirmed the absence of the benzoyl acetone fragment.

The ^{1}H NMR spectrum of compound (IV) displayed two doublets at δ 6.74 and 7.75 ppm, characteristic of para-disubstituted benzene rings, an imine proton at δ 8.60 ppm, and a singlet at δ 3.05 ppm corresponding to the N-methyl groups. The ^{13}C NMR spectrum showed signals at δ 40 ppm for the methyl carbons, quaternary carbons at δ 120 and 130 ppm, and the imine carbon at δ 160 ppm. For compound (V), the ^{1}H NMR spectrum showed multiplets at δ 6.94-7.68 ppm for the aromatic protons, an imine proton at δ 8.97 ppm, and a hydroxyl proton at δ 11.17 ppm, which disappeared upon D_2O exchange.

The proposed mechanism for this unprecedented transformation involves initial Schiff base formation between compound (II) and the aldehyde, followed by a retro-condensation reaction that releases the benzoyl acetone fragment as shown in scheme (2). This cleavage is likely driven by the formation of a highly stable conjugated hydrazone product, which is further stabilized by extensive electron delocalization. The electron-donating substituents on the aromatic aldehydes appear to facilitate this degradation-condensation sequence by stabilizing the intermediate carbocation or by enhancing the leaving group ability of the benzoyl acetone fragment.



Scheme (2): The proposed mechanism for formation of compound (IV)

The active methylene group of benzoyl acetone was exploited for azo coupling with the diazonium salt derived from 2,4-dichloroaniline. The azo coupling reaction proceeded smoothly, yielding the azo-benzoyl acetone derivative (2). The presence of the azo functionality not only introduces a chromophoric unit but also modulates the reactivity of the adjacent carbonyl groups through its electron-withdrawing effect.

The reaction of compound (2) with hydrazine hydrate was investigated under different molar ratios. Surprisingly, in all cases, the same product (VII) was obtained, indicating a highly regioselective transformation. The ^{1}H NMR spectrum of compound (VII) showed a singlet at δ 2.5 ppm corresponding to the methyl group, pyrazole and aromatic protons in the region δ 7.4-8.0 ppm, and an NH proton at δ 13.53 ppm, which disappeared upon D_2O exchange. The ^{13}C NMR spectrum was consistent with the proposed pyrazole structure.

The formation of a single product from this reaction can be rationalized by considering the directing effect of the azo group. The electron-withdrawing nature of the dichlorophenylazo substituent increases the electrophilicity of the adjacent carbonyl, directing the hydrazine attack to this position. Subsequent cyclization then proceeds through a favored pathway to give the pyrazole ring. The consistency of the product across all stoichiometric ratios suggests that the reaction is under kinetic control and that the intermediate formed after the first hydrazine addition is rapidly converted to the final product, preventing further reaction at the second carbonyl.

Microbiological Evaluation: The *in vitro* antibacterial activities of five synthesized compounds (I, II, V, VI, and VIII) were assessed against three clinically significant Gram-negative bacterial strains: *Escherichia coli*, *Klebsiella pneumoniae*, and *Salmonella* spp. The antimicrobial efficacy of these compounds was compared with that of standard antibiotic discs, including Kanamycin (K30),

Amikacin (AK30), Amoxycillin (AMC30), Ciprofloxacin (CIP30), Tetracycline (TE30), Cephalothin (CH30), and Rifampicin (R30), using the disc diffusion method.

As presented in Table 1 and Figure 1, compound (I) demonstrated the highest antibacterial potency among all tested compounds across the entire panel of bacterial strains. At a concentration of 5%, compound (I) produced inhibition zone diameters of 2.6 mm, 1.7 mm, and 1.3 mm against *E. coli*, *K. pneumoniae*, and *Salmonella* spp., respectively. Notably, compound (VII) exhibited selective antibacterial activity against *Salmonella* spp., yielding a maximum inhibition zone diameter of 2.8 mm at a 5% concentration (Figure 2). However, its activity was markedly reduced at a lower concentration (2.5%), with inhibition zones ranging from 0.5 to 1.2 mm. In contrast, compounds (II), (V), and (VI) displayed no detectable inhibitory effect against *Salmonella* spp. Furthermore, compounds (II), (V), and (VII) were ineffective against *K. pneumoniae*, as evidenced by the absence of inhibition zones.

The antibiotic susceptibility assay revealed considerable variation in the responses of the tested bacterial isolates to the standard antibiotics (Table 2, Figure 3). Among the isolates, *E. coli* exhibited the highest overall susceptibility. Ciprofloxacin produced the largest inhibition zone diameter (4.7 mm), followed by kanamycin (1.9 mm), amikacin (1.3 mm), and both tetracycline and cephalothin (1.0 mm each).

Conversely, *Salmonella* spp. displayed complete resistance to amoxicillin, tetracycline, cephalothin, and kanamycin, as indicated by the absence of inhibition zones surrounding the respective antibiotic discs. Additionally, amikacin exhibited only weak antibacterial activity against *Salmonella* spp., producing the smallest recorded inhibition zone diameter of 0.7 mm. Similarly, *K. pneumoniae* demonstrated resistance to multiple antibiotics, including amikacin, tetracycline, and cephalothin, with no detectable zones of inhibition. However, kanamycin showed moderate activity against this isolate, producing an inhibition zone of 1.5 mm, while amoxycillin and rifampicin each yielded zones of 1.0 mm.

In conclusion, compound (I) exhibited the most potent and broad-spectrum antibacterial activity among the synthesized derivatives, positioning it as a promising lead candidate for further development against Gram-negative bacterial pathogens. The susceptibility profiles of the tested organisms varied significantly depending on the antimicrobial agent, with *E. coli* being generally more susceptible, whereas *Salmonella* spp. and *K. pneumoniae* exhibited multidrug resistance patterns to several of the standard antibiotics (Figure 4).

Table (6): The effect of chemical compounds on the growth of some types of bacteria

Antibiotic (30 µg)	**inhibition zone (mm)**		
	Escherichia coli	***Klebsiella pneumoniae***	***Salmonella* spp**
Kanamycin (K)	1.9	1.5	0
Amikacin (AK)	1.3	1	0.7
Amoxycillin (AMC)	0	0	0
Ciprofloxacin (CIP)	4.7	0	1
Tetracycline (TE)	1	0	0
Cephalothin (CH)	1	0	0
Rifampicin (R)	0.9	1	1

Table (7): presents the inhibition zone diameters obtained from the antibiotic susceptibility test of the tested bacterial isolates

Control	**chemical compounds**	**Concentration Percentage %**	**inhibition zone (mm)**		
			Escherichia coli	***Klebsiella pneumoniae***	***Salmonella* spp**
$CHCl_3$	I	5	2.6	1.7	1.3
		2.5	2.2	1.5	1.2
		Control	0	0	0
	II	5	1.3	0	0
		2.5	1	0	0
		Control	0	0	0
	VI	5	0	1.8	0

		2.5	0	1.3	0
		Control	1	1.2	1
DMSO	V	5	0	0	0
		2.5	0	0	0
		Control	0	0	0
	VII	5	0	0	2.8
		2.5	0	0	0.5
		Control	0	0	0

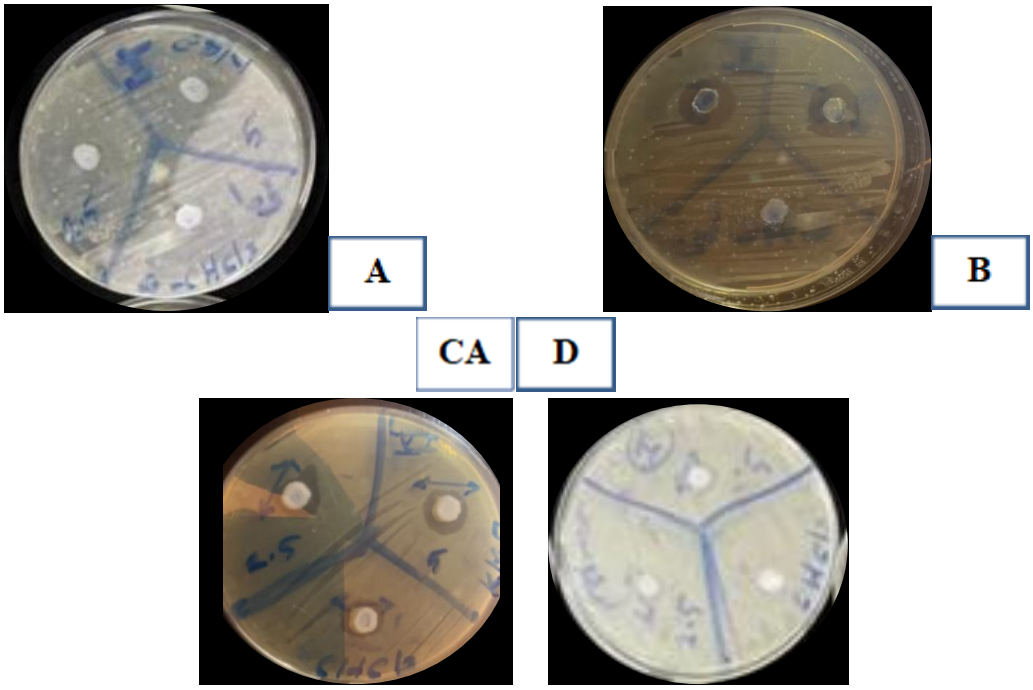


Figure (2): the largest inhibition zone diameters produced by compound I

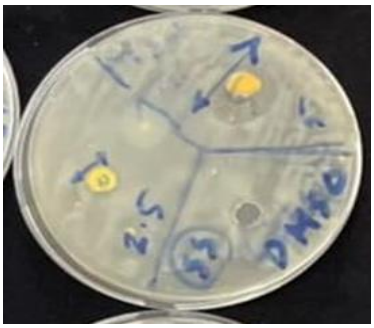


Figure (3): the inhibition zone diameters produced by compound IV dissolved in DMSO against Salmonella spp



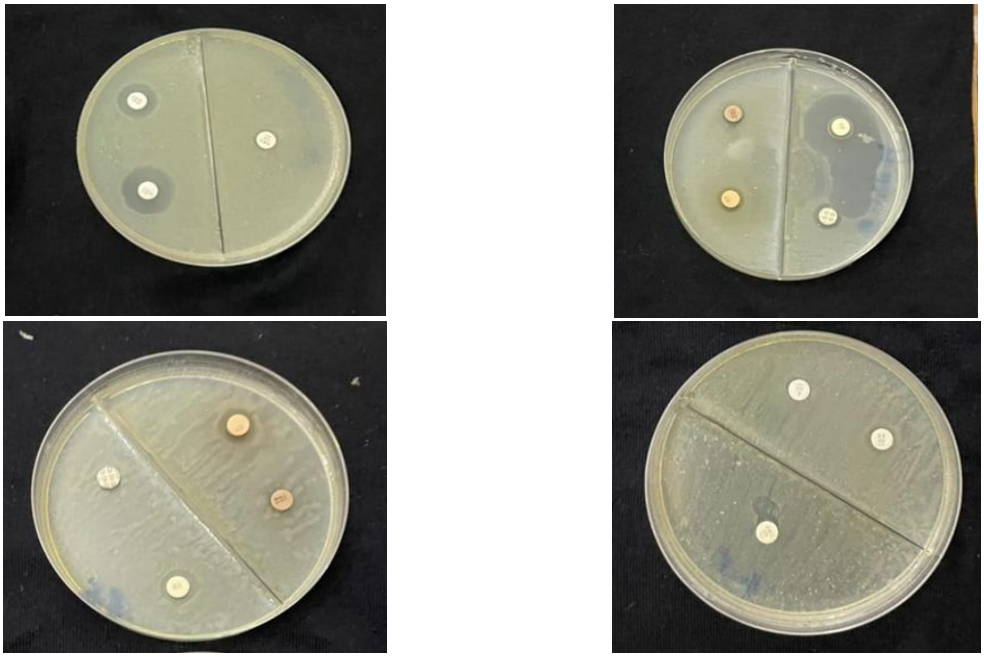


Figure (4): the inhibition zone diameters produced by the antibiotics against the Bacteria

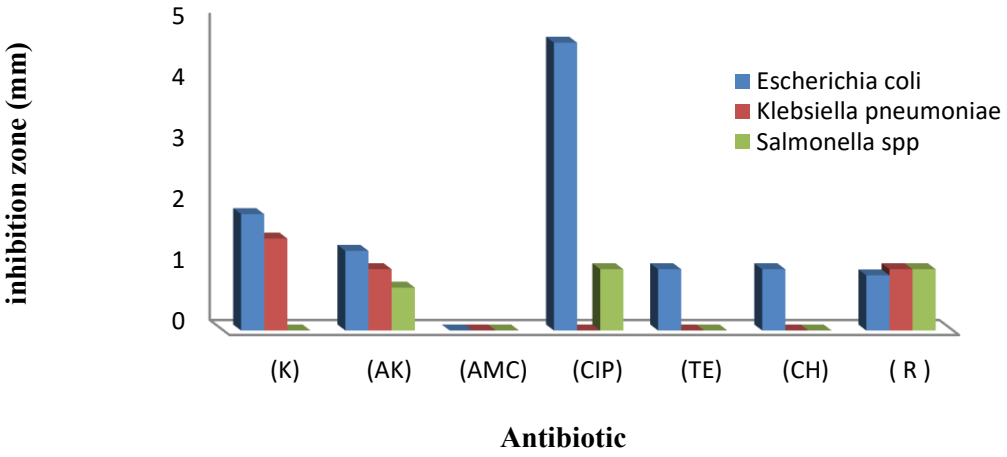


Figure (5): The inhibition zone diameters produced by the antibiotics against the Bacteria

Docking Protocol Validation and Binding Interactions:

Initially, the validation of the molecular docking protocol was carried out by redocking the co-crystallized reference ligand (Ref) back into the active site of *Klebsiella pneumoniae* dihydrofolate reductase (PDB ID: 4OR7). This procedure exhibited a strong binding affinity, yielding a docking score (S) of -7.891 kcal/mol alongside an RMSD value of 1.365 Å—safely beneath the conventional 2.0 Å validation threshold—thereby confirming the reproducibility, robustness, and accuracy of the MOE docking framework.

According to a detailed examination of the interactions, a compact network of non-covalent forces stabilizes the binding mode of Ref. This network is chiefly anchored via critical hydrogen donor bonds (2.75 Å, -7.4 kcal/mol; 3.00 Å, -8.0 kcal/mol) and multiple ionic contacts (2.75- 3.64 Å) through the vital catalytic residue ASP 27, along with extra stabilizing hydrogen bonds involving ALA 6 (3.09 Å), ILE 5 (3.00 Å), and ILE 94 (2.97 Å), plus a hydrophobic π-π stacking interaction with PHE 31 (4.06 Å).

Among the newly synthesized candidates (I, II, V, VI, and VII), Ligand VI displayed the top binding affinity (S=-7.167 kcal/mol, RMSD=1.666 Å), closely mirroring the reference compound's energy profile and securing stabilization through a π-H hydrophobic contact with THR 46 (4.28 Å). In addition, Ligand

VII exhibited notable binding capability (S=-6.244 kcal/mol, RMSD=1.568 Å), which was facilitated by dual π-H interactions involving THR 46 (3.99 Å) and PHE 31 (3.69 Å).

Conversely, moderate binding energies were recorded for compounds I (-5.166 kcal/mol), II (-5.741 kcal/mol), and V (-5.998 kcal/mol), which were driven by individual hydrogen bonds or hydrophobic π"-H" contacts with residues including ILE 94, ALA 6, ALA 7, ILE 14, and GLY 15.

Global reactivity descriptors:

Chemical reactivity descriptors were computed and compiled in Table 5. Data regarding EHOMO and ELUMO were acquired using GaussView [30]. Furthermore, findings concerning global hardness and softness—parameters intrinsically linked to the stability of a chemical system—demonstrate that Compound I possesses a higher hardness level relative to the remaining derivatives, as illustrated in Table 5. Additionally, Compound VII exhibits the smallest energy gap (ΔE=3.7239 eV), alongside a softness value superior to those recorded for compounds I, II, V, and VI. Collectively, these results confirm that Compound I is characterized by enhanced stability and reduced reactivity compared to the other compounds.

In terms of electronic chemical potential (μ), Compound II displays the highest value (μ=-2.6632 ev), followed sequentially by Compounds I, VII, and VI. These findings indicate that such derivatives are capable of efficiently exchanging electron density with their surrounding environment [31].

Based on the data presented in Table 7, Compound II can be classified as a strong nucleophile. Moreover, electrophilicity (ω) has emerged as a powerful metric for investigating the reactivity profiles of organic molecules capable of participating in polar reactions (26). Compound V recorded the maximum electrophilicity value (ω=3.4700 ev), whereas Compounds VI and VII exhibited elevated electrophilicity values (ω=3.1941 eV, 3.1534 ev) that surpass those calculated for Compounds I and II (ω=2.2369 ev, 1.7322 ev).

Conclusion:

The results presented in this study demonstrate that benzoyl acetone is a versatile precursor for the synthesis of diverse heterocyclic and azo compounds through regioselective transformations. The strategic use of different diamines, particularly hydrazine hydrate and ethylenediamine, under carefully controlled conditions allows for the selective formation of distinct product classes. The stoichiometry of hydrazine hydrate proved to be a critical determinant, with 1:1 or 2:1 ratio yielding the pyrazole product (I), while an excess amount diverted the reaction toward the hydrazone derivative (II). In contrast, the reactions with ethylenediamine were consistently selective across all proportions, affording a single product (VI). A particularly significant finding was the reactivity of compound (II), which underwent a novel and unprecedented cleavage of the benzoyl acetone moiety upon condensation with various aldehydes. This room-temperature, catalyst-free transformation efficiently produced Schiff bases (III, IV, V) in a short reaction time, presenting a departure from previously reported methodologies and offering a new, streamlined approach to these derivatives.

The antimicrobial evaluation identified compound (I) as the most promising antibacterial agent, exhibiting activity against all three tested Gram-negative pathogens. Compound (VII) demonstrated selective activity against Salmonella spp., while compound (VI) showed specificity toward K. pneumoniae. The structure-activity relationships revealed in this study provide valuable insights for the rational design of new antimicrobial agents based on the benzoyl acetone scaffold.

Collectively, these findings not only provide a comprehensive understanding of the factors governing the reactivity of benzoyl acetone with different diamines but also introduce a set of practical, rapid, and economical protocols for the synthesis of diverse bioactive heterocyclic compounds. The distinct reaction pathways discovered herein, particularly the unique degradation-condensation sequence for forming Schiff bases, open new avenues for the design and development of functionalized molecules with potential applications in medicinal chemistry and materials science.

Molecular docking analysis revealed that compound VI demonstrated the most favorable binding affinity among the investigated compounds, exhibiting a binding energy of −7.167 kcal/mol, while compound I displayed the least favorable binding affinity, with a binding energy of −5.166 kcal/mol.

the results obtained from global reactivity indices indicated that compound VII is the more reactive based on the HOMO – LUMO gap.

References:

1. Das, R., Kundu, T., & Basumatary, J. (2023). Visible light mediated organocatalytic dehydrogenative aza-coupling of 1,3-diones using aryldiazonium salts. RSC Advances, 13(5), 3147–3154. https://doi.org/10.1039/D2RA07807D
2. Hauser, C. R., & Walker, H. G., Jr. (1947). Condensation of certain esters by means of diethylaminomagnesium bromide. Journal of the American Chemical Society, 69(2), 295–297. https://doi.org/10.1021/ja01194a040
3. Rathke, M. W., & Deitch, J. (1971). The reaction of lithium ester enolates with acid chlorides: A convenient procedure for the preparation of β-keto esters. Tetrahedron Letters, 12(31), 2953–2956. https://doi.org/10.1016/S0040-4039(01)97034-0
4. Ried, W., & Höhne, W. (1954). Über heterocyclische Siebenringsysteme, III. Mitteil.: Synthesen einfacher 7-gliedriger Heterocyclen mit 2 Stickstoff-Atomen. Chemische Berichte, 87(12), 1811–1814. https://doi.org/10.1002/cber.19540871203
5. Yao, H. C. (1964). Azo-hydrazone conversion. II. The coupling of diazonium ion with β-diketones. The Journal of Organic Chemistry, 29(10), 2959–2963. https://doi.org/10.1021/jo01033a037
6. Alinezhad, H., Tajbakhsh, M., Sarkati, M. N., & Zare, M. (2016). Nano-SiO_2 catalyzed synthesis of β-enaminones under solvent-free conditions. Monatshefte für Chemie—Chemical Monthly, 147, 1591–1596. https://doi.org/10.1007/s00706-016-1654-5
7. Skopenko, V. V., Amirkhanov, V. M., Sliva, T. Yu., Vasilchenko, I. S., Anpilova, E. L., & Garnovskii, A. D. (2004). Various types of metal complexes based on chelating β-diketones and their structural analogues. Russian Chemical Reviews, 73(8), 737–752. https://doi.org/10.1070/RC2004v073n08ABEH000909
8. Claisen, L., & Lowman, O. (1887). Ueber eine neue Bildungsweise des Benzoylessigäthers. Berichte der Deutschen Chemischen Gesellschaft, 20(1), 651–654. https://doi.org/10.1002/cber.188702001149
9. Tahir, M. N., Kausar, N., Abbas, A., & Murtaza, S. (2015). Synthesis, characterization and biological evaluation of Schiff bases of propanedihydrazide. American-Eurasian Journal of Agricultural & Environmental Sciences, 15(12), 2479–2483. https://doi.org/10.5829/idosi.aejaes.2015.15.12.12831
10. Backes, G. L., Neumann, D. M., & Jursic, B. S. (2014). Synthesis and antifungal activity of substituted salicylaldehyde hydrazones, hydrazides and sulfohydrazides. Bioorganic & Medicinal Chemistry, 22(16), 4629–4636. https://doi.org/10.1016/j.bmc.2014.07.022
11. Bustos, C., Alvarez-Thon, L., Molins, E., Moreno-Villoslada, I., Vallejos-Contreras, G., Sánchez, C., Zarate, X., Mac-Leod Carey, D., & Schott, E. (2018). Tuning the molecular/electronic structure of new substituted pyrazoles: Synthesis, biological trials, theoretical approaches and Hammett correlations. Journal of Molecular Structure, 1171, 349–361. https://doi.org/10.1016/j.molstruc.2018.05.088
12. Eldeab, H. A. (2019). Green synthetic approach and antimicrobial evaluation for some novel pyridyl benzoate derivatives. Russian Journal of Organic Chemistry, 55(7), 1034–1040. https://doi.org/10.1134/S1070428019070200
13. Jain, M., Nehra, S., Trivedi, P. C., & Singh, R. V. (2002). Nematicidal, fungicidal and bactericidal activities of manganese (II) complexes with heterocyclic sulphonamide imines. Metal-Based Drugs, 9(1–2), 53–60. https://doi.org/10.1155/MBD.2002.53
14. Prakash, A., & Adhikari, D. (2011). Application of Schiff bases and their metal complexes—A review. International Journal of ChemTech Research, 3(4), 1891–1896.
15. Popiołek, Ł. (2021). Updated information on antimicrobial activity of hydrazide-hydrazones. International Journal of Molecular Sciences, 22(17), Article 9389. https://doi.org/10.3390/ijms22179389
16. Karrouchi, K., Radi, S., Ramli, Y., Taoufik, J., Mabkhot, Y. N., Al-Aizari, F. A., & Ansar, M. (2018). Synthesis and pharmacological activities of pyrazole derivatives: A review. Molecules, 23(1), Article 134. https://doi.org/10.3390/molecules23010134
17. Kajal, A., Bala, S., Sharma, N., Kamboj, S., & Saini, V. (2014). Therapeutic potential of hydrazones as anti-inflammatory agents. International Journal of Medicinal Chemistry, 2014, Article 761030. https://doi.org/10.1155/2014/761030

18. Perez, C., Paul, M., & Bazerque, P. (1990). An antibiotic assay by the agar well diffusion method. Acta Biologiae et Medicinae Experimentalis, 15, 113–115.
19. Clinical and Laboratory Standards Institute. (2020). Performance standards for antimicrobial susceptibility testing (30th ed.; CLSI supplement M100).
20. Chemical Computing Group ULC. (2024). Molecular Operating Environment (MOE) (Version 2024.0601) [Computer software].
21. Becke, A. D. (1997). Density-functional thermochemistry. V. Systematic optimization of exchange-correlation functionals. The Journal of Chemical Physics, 107(20), 8554–8560. https://doi.org/10.1063/1.475007
22. Hehre, W. J., Ditchfield, R., & Pople, J. A. (1972). Self-consistent molecular orbital methods. XII. Further extensions of Gaussian-type basis sets for use in molecular orbital studies of organic molecules. The Journal of Chemical Physics, 56, 2257–2261. https://doi.org/10.1063/1.1677527
23. Frisch, M. J., Trucks, G. W., Schlegel, H. B., Scuseria, G. E., Robb, M. A., Cheeseman, J. R., Scalmani, G., Barone, V., Mennucci, B., Petersson, G. A., Nakatsuji, H., Caricato, M., Li, X., Hratchian, H. P., Izmaylov, A. F., Bloino, J., Zheng, G., Sonnenberg, J. L., Hada, M., … Fox, D. J. (2009). Gaussian 09 (Revision A.02) [Computer software]. Gaussian, Inc.
24. Cavalli, A., Carloni, P., & Recanatini, M. (2006). Target-related applications of first principles quantum chemical methods in drug design. Chemical Reviews, 106(9), 3497–3519. https://doi.org/10.1021/cr050579p
25. Lamb, K. M., Lombardo, M. N., Alverson, J., Priestley, N. D., Wright, D. L., & Anderson, A. C. (2014). Crystal structures of Klebsiella pneumoniae dihydrofolate reductase bound to propargyl-linked antifolates reveal features for potency and selectivity. Antimicrobial Agents and Chemotherapy, 58(12), 7484–7491. https://doi.org/10.1128/AAC.03555-14
26. Domingo, L. R., Ríos-Gutiérrez, M., & Pérez, P. (2016). Applications of the conceptual density functional theory indices to organic chemistry reactivity. Molecules, 21(6), Article 748. https://doi.org/10.3390/molecules21060748
27. Kellenberger, E., Rodrigo, J., Muller, P., & Rognan, D. (2004). Comparative evaluation of eight docking tools for docking and virtual screening accuracy. Proteins: Structure, Function, and Bioinformatics, 57(2), 225–242. https://doi.org/10.1002/prot.20149
28. Shahab, S., Hajikolaee, F. H., Filippovich, L., Darroudi, M., Loiko, V. A., Kumar, R., & Yousefzadeh Borzehandani, M. (2016). Molecular structure and UV–Vis spectral analysis of new synthesized azo dyes for application in polarizing films. Dyes and Pigments, 129, 9–17. https://doi.org/10.1016/j.dyepig.2016.02.003
29. Del Re, G., Berthier, G., & Serre, J. (1980). Electronic states of molecules and atom clusters: Foundations and prospects of semiempirical methods (Lecture Notes in Chemistry, Vol. 13). Springer-Verlag. https://doi.org/10.1007/978-3-642-93134-5
30. Dennington, R., Keith, T. A., & Millam, J. M. (2016). GaussView (Version 6.0) [Computer software]. Semichem Inc.
31. Azarhazin, E., Izadyar, M., & Housaindokht, M. R. (2019). Drug–DNA interaction: A joint DFT-D3/MD study on safranal as an anticancer and DNA nanostructure model. Canadian Journal of Chemistry, 97(2), 120–130. https://doi.org/10.1139/cjc-2018-0126